UKACC International Conference on Control 2012
Cardiff, UK, 3-5 September 2012

A decentralised control strategy for formation flight of unmanned aerial vehicles

Aolei Yang, Wasif Naeem, George W. Irwin, and Kang Li
School of Electronics, Electrical Engineering and Computer Science
Queen's University Belfast, BT9 5AH, UK.
Email: ayang02@qub.ac.uk, w.naeem@qub.ac.uk, g.irwin@qub.ac.uk, k.li@qub.ac.uk

***Abstract*—This paper presents a methodology to solve formation flight problem for unmanned aerial vehicles (UAVs). It employs a unique "*extension-decomposition-aggregation*" scheme to transform the overall complex formation control problem to a group of sub-problems. The decentralised formation longitudinal and lateral autopilots are designed to support the implementation of the formation flight and manoeuvring of UAVs. Simulation studies have been carried out to verify the performance and effectiveness of the presented cooperative flight strategy.**

***Index Terms*—Cooperative flight; Decentralised control; Formation autopilot; Unmanned aerial vehicle**

I. Introduction

Research in cooperative flight control of multi-aircraft systems has attracted growing interest in recent years. After NASA launched the Autonomous Formation Flight (AFF) program, extensive research and development work has been carried out. One of the experiments was conducted by Dryden Flight Research Center, which demonstrated that an F/A-18 flying in the wingtip vortex behind another F/A-18 exhibited a 14% fuel savings [1]. In addition, in [2], the authors presented the benefits that birds "V" shape formation flying brings to energy saving compared to isolated flying, because of the reduction in induced flying drag. Further, its implications are very significant, not just for fuel and energy saving but for other future applications in civilian and military domains. For instance, formation flight can be used to handle increase in air traffic around airports through civil aeroplane formation taking-off and landing to increase use efficiency of airport runway, and applications in military field include aerial refuelling, aircraft logistics, air formation patrol, and carrier landing systems.

Successful formation flight requires the solution of the formation control problem. A number of approaches have been proposed in the literature. For instance, in [3] and [4], the decentralised behaviour-based approach which was inspired by the study of animal behaviour was applied to a group of mobile vehicles. In [5], the leader-following strategy was employed, which has been widely used to deal with the aircraft formation flight control. Virtual structure approach for synchronising UAV position tracking control and for maintaining formation geometry was presented in [6]. Further, the authors have introduced the extension-decomposition-aggregation (EDA) formation control strategy in [7] to translate the complex formation control problem into a group of sub-problems which are simpler to solve. There, the EDA scheme was applied to the formation control of a point mass robot in the horizontal plane.

In this paper, the EDA strategy is further extended and applied to the complex cooperative flight control of UAVs. A nonlinear *Aerosonde* UAV model is linearised about specific trim conditions, and the multivariable H_∞ control methodology based on linear matrix inequalities (LMI) is then employed to design the longitudinal and lateral formation controllers to maintain the corresponding formation stability. Additionally, proportional-integral (PI) compensators are designed to eliminate steady-state formation errors. Simulation studies showing formation manoeuvres have been performed to demonstrate the effectiveness of the proposed method and the formation stability.

This paper is organised as follows. Section II presents the problem formulation and preliminaries. Section III proposes the EDA formation control methodology, whilst Section IV describes the decentralised longitudinal and lateral formation autopilots design. Section V reports the implementation and simulation results. Finally, concluding remarks and suggestions for future work are provided in Section VI.

II. Problem formulation and preliminaries

Consider a group of three UAVs flying in a specified formation as depicted in Fig. 1. A reference vehicle (RV) in the group can be selected by a consensus between the UAVs. Note that the RV is different from the leader vehicle in the leader-following approach, since it is mainly used to define the local formation coordinate system (LFCS), which is a convenient way of describing a formation, a simple illustration being shown in Fig. 1.

In contrast to the earth axes frame (X_E, Y_E, Z_E) and the fixed body axes frame (X_B, Y_B, Z_B), the LFCS-axes, (X_L, Y_L, Z_L) are always aligned with the vehicle body axes of the RV. This implies that the LFCS axes always vary with the RV's position and direction. From Fig. 1, the position vector of the i^{th} vehicle in the LFCS is defined as $\mathbf{p}_{Li} = [p_{Lix}, p_{Liy}, p_{Liz}]$, and the desired formation can then be mathematically expressed as $F_d = [\mathbf{p}_{L1}; \mathbf{p}_{L2}; \cdots; \mathbf{p}_{LN}]$, where L represents the LFCS and N is the number of vehicles in the formation.

However, it is not enough to describe a formation by only defining the position in the LFCS, since the motion of UAVs in 3D has six degree-of-freedom (6-DOF) defining the

978-1-4673-1558-6/12/$31.00 ©2012 IEEE

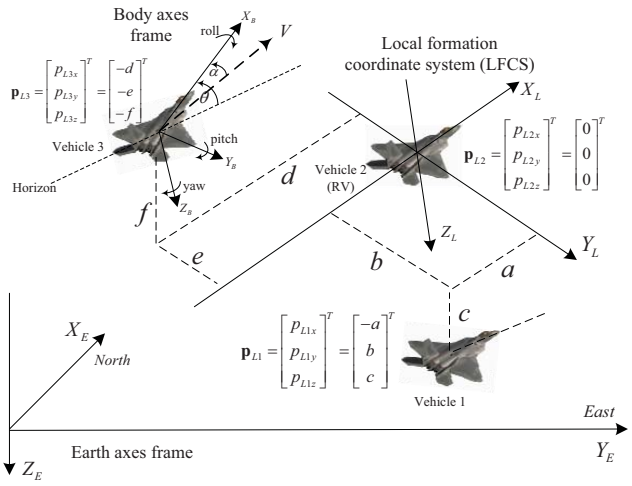

Fig. 1. Local formation coordinate system

positions and attitudes. Thus, a complete formation definition in Euclidean space is given by,

$$F_d = [\mathbf{p}_{L1}; \mathbf{p}_{L2}; \cdots; \mathbf{p}_{LN}]$$
$$\tilde{\mathbf{x}}_i = [\phi_i, \theta_i, \psi_i, \cdots]^T : i = 1, 2, \cdots, N. \quad (1)$$

where ϕ_i, θ_i and ψ_i are the roll, pitch and yaw angles respectively constituting the attitude of the i^{th} individual vehicle. Note that the above attitude angles are just partial elements of the state vector $\tilde{\mathbf{x}}_i$ of the i^{th} vehicle. when a formation change is needed, $\tilde{\mathbf{x}}_i$ must generally be regulated by the formation control algorithm. Subsequently, all vehicles within the group will achieve their new desired relative distances. This implies that stabilising relative positions in a formation is a sufficient condition to achieve equal attitude angles. Thus, the primary function of formation control is to maintain the stability of the relative positions by controlling the states of each vehicle (such as the attitude angles above).

III. Formation Control Methodology

A. Novel strategy for decentralised formation control

It has been recognised that complex systems can be decomposed into subsystems of lower dimensionality, and those individual subsystem solutions are then combined in some way to provide an overall system response. Motivated by this idea, the EDA scheme proposed in [7] is described in detail here, and Fig. 2 shows the overall process.

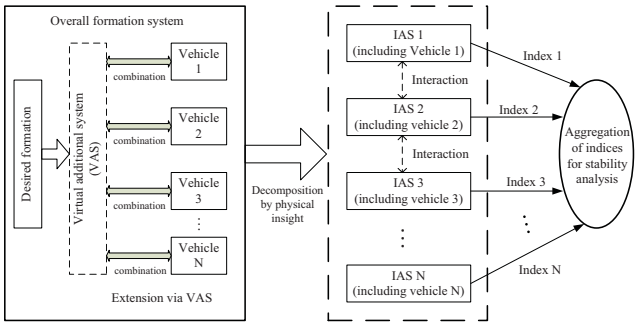

Fig. 2. Process of the extension-decomposition-aggregation

For the case of multi-vehicle formation control, each vehicle is a separate entity in the formation space, i.e. there is generally no explicit relationship among the vehicles to represent their formation statuses. The strategy here is to introduce a *virtual* additional system (VAS), which has three main functions: (1) to build a relationship between the isolated vehicles leading to a new overall vehicle formation control system, (2) to involve the desired formation variables or parameters in the overall formation control system, which could be combined with the related individual vehicle model, and (3) to support the subsequent decomposition, and to simplify stability analysis of the overall formation. Note that the VAS is merely an algorithm to act as an "interaction bridge" providing each vehicle with the capability of sensing its local-formation states, which can then be used in the formation control design.

Since the overall formation system involving many variables is difficult to handle as a whole, it is natural to decompose it into several local-formation subsystems. However, it is noted that there is no general systematic procedure for decomposing such a complex dynamical system. Here, using physical insight the overall formation system is decomposed into N individual subsystems, each being called an individual augmented subsystem (IAS) since it combines the individual vehicle model and the local-formation variables. Thus, the initial overall complex formation control problem can now be redefined in terms of stability and set-point tracking for all the decomposed IASs.

In order to analyse the stability of the overall formation, a viable idea is to select a scalar Lyapunov function as an index to represent the stability of each IAS. These indices are then aggregated to mathematically analyse the stability of the overall formation system through the Lyapunov theory. This also brings about a considerable reduction in the dimensionality of the formation stability problem. However, the focus in this paper is on the performance of the proposed formation control system and therefore the stability analysis is not shown here.

B. A candidate VAS: coupled multiple pendulums

To meet the requirements of the additional system, a virtual multiple-inverted-pendulum system was employed in the original algorithm [7]. However, here a virtual coupled-multiple-pendulum system (CMP) shown in Fig. 3 is used to demonstrate the flexibility of the proposed approach. Here, the

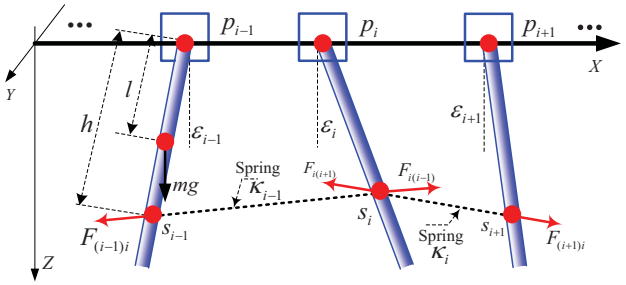

Fig. 3. Coupled multiple pendulums system

CMP consists of N cart-mounted pendulums coupled by $N-1$

springs, and the model of the individual pendulum within the CMP is given by (2),

$$J\ddot{\varepsilon} = -B_c\dot{\varepsilon} - mla\cdot\cos\varepsilon - mgl\sin\varepsilon + W \tag{2}$$

where $J = I + ml^2 = 4ml^2/3$, $I = ml^2/3$ is the inertial moment of pendulum, ε stands for the deflection angle of each pendulum, B_c is the viscous damping constant at the pivot point, a represents the acceleration, l is the length from the pivot to the gravity centre, m and g represent the mass and the gravitational constant respectively, and W is the resultant torque from the connected springs.

In Fig. 3, each cart of the CMP system can be associated with a vehicle in the formation. The spring connecting two pendulums corresponds to the communication channel between two vehicles, where the magnitude of the torque from the spring force depends on the spring coefficient (k_s), the free or natural length (l_{κ_i}), and the relative distances between the vehicles. Based on these associations, one approach for constructing the relationship is to consider l_{κ_i} as the desired formation parameter. Thus, if a formation is disturbed, the force or torque which is caused by the springs must then impact the pendulums, resulting in a change in their deflection angles, ε_i. This implies that the variation of ε_i is a reflection of the formation error. Thus, the aim of the individual formation control for each IAS is to regulate the deflection angle by manipulating the vehicle states. This will automatically cause the spring to return to its balanced state, i.e. the formation becomes stable. If all the springs return to their natural states or all the deflection angles are equal to zero, this in turn implies that the formation is stable with zero formation error.

Since the CMP is a virtual system, its parameters can be altered by the control algorithm according to the physical dynamics and engineering design requirements of the formation. For example, if the natural length of the springs are dynamically re-defined, the overall vehicle formation will likewise be changed. One of the most interesting aspects of this strategy is that it can be applied to handle vehicle collisions and the desertion problem, both of which are of prime importance in the motion of multiple vehicles. However, this is not discussed here due to lack of space. Recalling the EDA scheme shown in Fig. 2, the overall system is then partitioned or decomposed at the spring positions to obtain the IASs as explained in the next section.

IV. Decentralised formation autopilot design

A. Modelling of longitudinal and lateral IASs

Following the standard convention, the 6-DOF aircraft dynamics is approximately decomposed into its longitudinal and lateral components. The longitudinal motion occurs within the plane of symmetry of the aircraft, whereas the lateral-directional motion occurs outside of this plane of symmetry. Based on this separated characteristics and the scheme of EDA, the longitudinal IAS and the lateral IAS can in general be expressed by (3) and (4) respectively.

$$\begin{cases} \dot{\tilde{\mathbf{x}}}_{long} = f(\tilde{\mathbf{x}}_{long}, \delta_{long}) \\ \ddot{\varepsilon}_{long} = -\frac{B_c}{J}\dot{\varepsilon}_{long} - \frac{mgl}{J}\sin\varepsilon_{long} - \frac{ml}{J}a_{long}\cdot\cos\varepsilon_{long} + \frac{1}{J}\cdot W_{long} \end{cases} \tag{3}$$

$$\begin{cases} \dot{\tilde{\mathbf{x}}}_{lat} = g(\tilde{\mathbf{x}}_{lat}, \delta_{lat}) \\ \ddot{\varepsilon}_{lat} = -\frac{B_c}{J}\dot{\varepsilon}_{lat} - \frac{mgl}{J}\sin\varepsilon_{lat} - \frac{ml}{J}a_{lat}\cdot\cos\varepsilon_{lat} + \frac{1}{J}\cdot W_{lat} \end{cases} \tag{4}$$

where $\tilde{\mathbf{x}}_{long}$, $\tilde{\mathbf{x}}_{lat}$ are the state vectors of the longitudinal and lateral dynamics, δ_{long}, δ_{lat} are their input vectors, $f(\cdot)$ and $g(\cdot)$ are the analytic functions modelling the dynamics of an UAV, ε_{long} and ε_{lat} are considered as the variables reflecting their local-formation errors, and a_{long} and a_{lat} are referred to as the longitudinal and lateral accelerations respectively in the inertial reference system.

The designed control framework of an individual aircraft formation system is illustrated in Fig. 4. Here, each plant

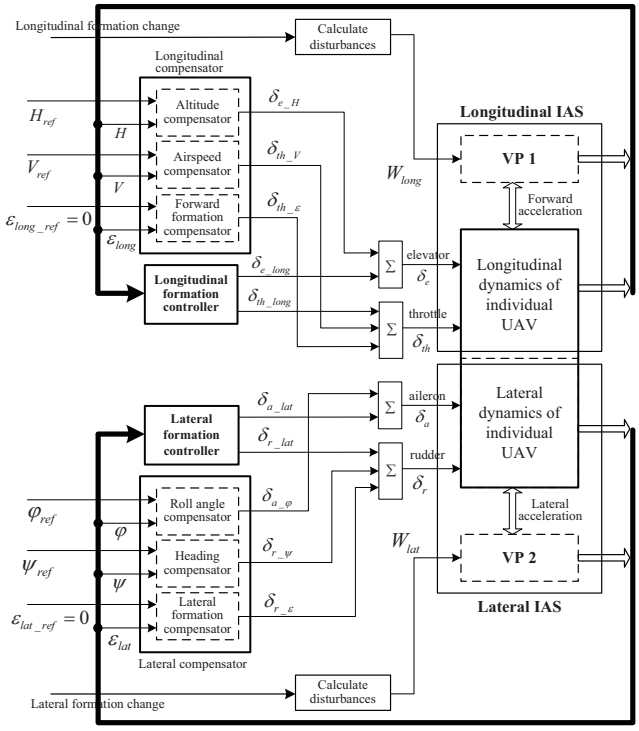

Fig. 4. Longitudinal and lateral autopilots framework

or so-called longitudinal IAS is generated by combining the longitudinal model with a virtual pendulum (VP) system, and the lateral IAS is obtained likewise. The exogenous inputs W_{long} and W_{lat} are derived from the longitudinal and lateral formation change or error, and are assumed to be *bounded disturbances* to the IASs.

The nonlinear models of the longitudinal and lateral IASs in (3) and (4) can be generally linearised about some specific trim conditions of the aircraft, into corresponding reduced-order state-space equations as shown in (5),

$$\begin{aligned} \dot{\mathbf{x}}_{long} &= A_{long}\mathbf{x}_{long} + B_{1\_long}\mathbf{W}_{long} + B_{2\_long}\mathbf{u}_{long} \\ \dot{\mathbf{x}}_{lat} &= A_{lat}\mathbf{x}_{lat} + B_{1\_lat}\mathbf{W}_{lat} + B_{2\_lat}\mathbf{u}_{lat} \end{aligned} \tag{5}$$

where $\mathbf{x}_{long} = [\tilde{\mathbf{x}}_{long}, \varepsilon_{long}, \dot{\varepsilon}_{long}]^T$ and $\mathbf{x}_{lat} = [\tilde{\mathbf{x}}_{lat}, \varepsilon_{lat}, \dot{\varepsilon}_{lat}]^T$ are the states of the longitudinal and lateral IASs respectively,

which are the augmented vectors from the vehicle states $\tilde{\mathbf{x}}_{long}$ and $\tilde{\mathbf{x}}_{lat}$. Similarly, $\mathbf{W}_{long}$ and $\mathbf{W}_{lat}$ are augmented vectors from W_{long} and W_{lat} respectively, whereas $\mathbf{u}_{long}$ and $\mathbf{u}_{lat}$ correspond to the control input vectors in the longitudinal and lateral directions.

B. Lateral formation autopilot design

For the lateral formation autopilot, the lateral formation motion in the (X_L, Y_L) plane is considered. As shown in Fig. 4, the proposed lateral formation autopilot consists of two components: the multivariable *lateral formation controller* and the *lateral compensators*. Here, the former is designed by using the LMI-based H_∞ robust control methodology [8], [9], [10], to compute the control signals (δ_{a_lat} and δ_{r_lat}), maintain the stability of the lateral IASs and reject the disturbances ($\mathbf{W}_{lat}$). However, it is noted that although these controllers maintain the stability of the lateral formation, zero steady-state formation error cannot be guarantee because of the system type. This is why PI-based lateral compensator given by (6) is supplemented for eliminating this error,

$$D(s) = K_p(1 + K_i/s) \tag{6}$$

where K_p and K_i are the proportional and integral parameters respectively, which are individually tuned for each of the roll, heading and lateral formation compensators.

Since the convergence of the roll and heading angles is a necessary condition for the stability of the overall formation system, the roll and heading compensators guarantee the roll and heading angles to asymptotically converge to ϕ_{ref} and ψ_{ref} respectively. The nominal value of ϕ_{ref} is usually set to zero during normal operation, whereas ψ_{ref} depends on vehicle's particular role in the formation. For instance, if the current vehicle is RV, ψ_{ref} can be calculated by a guidance algorithm, otherwise it should be the same as the heading angle of RV (ψ_{RV}). In addition, since the local-formation variable, ε_{lat}, is a reflection of the lateral formation change, the respective formation compensator is also required to converge ε_{lat} to ε_{lat_ref} which should be regulated to zero to ensure no steady-state formation error.

As shown in Fig. 4, the resultant of the complete inputs, δ_a and δ_r, for the lateral dynamics can be expressed by (7).

$$\begin{aligned} \delta_a &= \delta_{a\_lat} + \delta_{a\_\varphi} \\ \delta_r &= \delta_{r\_lat} + \delta_{r\_\psi} + \delta_{r\_\varepsilon} \end{aligned} \tag{7}$$

These control signals can then drive the individual UAV to maintain the stability of the lateral formation and compensate the steady-state lateral formation error.

C. Longitudinal formation autopilot design

The longitudinal formation autopilot deals with the longitudinal formation motion in the (X_L, Z_L) plane. It is generally more complicated than the lateral formation autopilot because the airspeed plays a significant role in different stages of the flight, such as take-off, climb/descend and altitude hold stages. The designed strategy here is that the *formation altitude steady-state error* is regulated by the pitch angle, and the *forward formation steady-state error* is eliminated by regulating the airspeed.

In Fig. 4, the longitudinal formation autopilot consist of two components: the *longitudinal formation controller* and the *longitudinal compensators*. The former can be also developed by using the LMI-based H_∞ control methodology to compute the control signals (δ_{e_long} and δ_{th_long}) to guarantee the stability of the longitudinal formation, and the latter is employed to eliminate the steady-state errors of the altitude (H), the airspeed (V) and forward formation (ε_{long}). The related compensators have the same structure as (6), where K_p and K_i are separately designed for each variable. The resultant control signals, δ_e and δ_{th}, of the longitudinal formation autopilot are then calculated by (8).

$$\begin{aligned} \delta_e &= \delta_{e\_long} + \delta_{e\_H} \\ \delta_{th} &= \delta_{th\_long} + \delta_{th\_V} + \delta_{th\_\varepsilon} \end{aligned} \tag{8}$$

These control inputs can then maintain the stability of the longitudinal formation in addition to compensating for the longitudinal steady-state formation error.

V. Implementation and Simulations

A. Implementation of linear longitudinal and lateral IASs

The performance of the proposed methodology was evaluated by using the 6-DOF *Aerosonde* UAV nonlinear simulink model [11]. The autonomous *Aerosonde* has a length of $1.74\,m$, a wingspan of $2.87\,m$, maximum payload capacity of $5\,kg$ and endurance of up to $30\,hours$. It was designed for applications including long-range weather data acquisition and reconnaissance over oceanic and remote areas.

In this paper, the IAS models were evaluated by trimming the *Aerosonde* model. The trim condition is chosen as: $V = 26\,m/s$, initial $H = 800\,m$, $\phi = 0\,rad$ and fuel mass is $2\,kg$. The parameter values of CMP system are heuristically chosen as: $m = 50\,kg$, $g = 9.81\,m/s^2$, $l = h = 0.3\,m$, $J = (4/3)ml^2 = 6\,kg\cdot m^2$, $B_c = 12\,N\cdot s/m$, $k_s = 0.1\,N/s$, but can be related to the dynamics of the physical system to be controlled. Furthermore, the relevant symbols representing the states, inputs and outputs of the longitudinal and lateral IASs are given in Table I.

TABLE I
Relevant symbols of *Aerosonde* linear model

Variable	Symbol	Variable	Symbol
Longitudinal velocity	u	Airspeed	V
Lateral velocity	v	Sideslip angle	β
Normal velocity	w	Angle of attack	α
Roll angle	ϕ	Roll rate	p
Pitch angle	θ	Pitch rate	q
Yaw angle	ψ	Yaw rate	r
Altitude	H	Engine rotation speed	ω
Longitudinal formation variable	ε_{long}	Lateral formation variable	ε_{lat}
Elevator deflection	δ_e	Throttle deflection	δ_{th}
Aileron deflection	δ_a	Rudder deflection	δ_r

Specifically, the resulting dynamic equations of the longitudinal IAS are written as (9), which are obtained from the trimming of (3).

$$\begin{aligned} \dot{\mathbf{x}}_{long} &= A_{long}\mathbf{x}_{long} + B_{1\_long}\mathbf{W}_{long} + B_{2\_long}\mathbf{u}_{long} \\ \mathbf{y}_{long} &= C_{long}\mathbf{x}_{long} + D_{1\_long}\mathbf{W}_{long} + D_{2\_long}\mathbf{u}_{long} \end{aligned} \tag{9}$$

where $\mathbf{x}_{long} = [u, w, q, \theta, H, \omega, \varepsilon_{long}, \dot{\varepsilon}_{long}]^T$, $\mathbf{u}_{long} = [\delta_e, \delta_{th}]^T$, and $\mathbf{y}_{long} = [V, \alpha, q, \theta, H, \varepsilon_{long}, \dot{\varepsilon}_{long}]^T$ represent the state, input, and output vectors respectively. The resulting matrices are given by (10).

$$
\begin{aligned}
A_{long} &= \begin{bmatrix}
-0.23 & 0.51 & -1.19 & -9.80 & 0 & 0.01 & 0 & 0 \\
-0.55 & -4.38 & 25.39 & -0.46 & 0 & 0 & 0 & 0 \\
0.41 & -4.73 & -5.06 & 0 & 0 & 0.01 & 0 & 0 \\
0 & 0 & 1 & 0 & 0 & 0 & 0 & 0 \\
0.05 & -1.00 & 0 & 26.00 & 0 & 0 & 0 & 0 \\
33.97 & 1.58 & 0 & 0 & -0.05 & -3.13 & 0 & 0 \\
0 & 0 & 0 & 0 & 0 & 0 & 0 & 1 \\
-0.65 & 0.76 & -0.02 & -24.53 & 0 & 0.03 & -24.5 & -2
\end{bmatrix} \\
B_{1\_long} &= \begin{bmatrix} 0 & 0 & 0 & 0 & 0 & 0 & 0 & 0.1667 \end{bmatrix}^T \\
B_{2\_long} &= \begin{bmatrix} 0.35 & -2.60 & -35.90 & 0 & 0 & 0 & 0 & 0.59 \\ 0 & 0 & 0 & 0 & 0 & 346.5 & 0 & 0 \end{bmatrix}^T \\
C_{long} &= \begin{bmatrix}
0.9989 & 0.0466 & 0 & 0 & 0 & 0 & 0 & 0 \\
-0.0018 & 0.0384 & 0 & 0 & 0 & 0 & 0 & 0 \\
0 & 0 & 1 & 0 & 0 & 0 & 0 & 0 \\
0 & 0 & 0 & 1 & 0 & 0 & 0 & 0 \\
0 & 0 & 0 & 0 & 1 & 0 & 0 & 0 \\
0 & 0 & 0 & 0 & 0 & 1 & 0 & 0 \\
0 & 0 & 0 & 0 & 0 & 0 & 1 & 0 \\
0 & 0 & 0 & 0 & 0 & 0 & 0 & 1
\end{bmatrix} \\
D_{1\_long} &= [0]_{8\times 1}, D_{2\_long} = [0]_{8\times 2}
\end{aligned}
\tag{10}
$$

Similarly, the state-space equations of the lateral IAS are expressed as (11), which were achieved by trimming of (4),

$$
\begin{aligned}
\dot{\mathbf{x}}_{lat} &= A_{long}\mathbf{x}_{lat} + B_{1\_lat}\mathbf{W}_{lat} + B_{2\_lat}\mathbf{u}_{lat} \\
\mathbf{y}_{lat} &= C_{lat}\mathbf{x}_{lat} + D_{1\_lat}\mathbf{W}_{lat} + D_{2\_lat}\mathbf{u}_{lat}
\end{aligned}
\tag{11}
$$

where $\mathbf{x}_{lat} = [v, p, r, \phi, \psi, \varepsilon_{lat}, \dot{\varepsilon}_{lat}]^T$, $\mathbf{u}_{lat} = [\delta_a, \delta_r]^T$, and $\mathbf{y}_{lat} = [\beta, p, r, \phi, \psi, \varepsilon_{lat}, \dot{\varepsilon}_{lat}]^T$. Their resulting matrices are given by (12).

$$
\begin{aligned}
A_{lat} &= \begin{bmatrix}
-0.68 & 1.21 & -25.97 & 9.80 & 0 & 0 & 0 \\
-4.47 & -21.99 & 10.58 & 0 & 0 & 0 & 0 \\
0.72 & -2.85 & -1.11 & 0 & 0 & 0 & 0 \\
0 & 1 & 0.05 & 0 & 0 & 0 & 0 \\
0 & 0 & 1.00 & 0 & 0 & 0 & 0 \\
0 & 0 & 0 & 0 & 0 & 0 & 1 \\
-1.69 & 0 & 0 & 0 & 0 & -24.53 & -2
\end{bmatrix} \\
B_{1\_lat} &= \begin{bmatrix} 0 & 0 & 0 & 0 & 0 & 0 & 0.1667 \end{bmatrix}^T \\
B_{2\_lat} &= \begin{bmatrix} -1.51 & -132.34 & -5.22 & 0 & 0 & 0 & -3.77 \\ 3.85 & 2.38 & -24.31 & 0 & 0 & 0 & 9.62 \end{bmatrix}^T \\
C_{lat} &= diag(0.0385, 1, 1, 1, 1, 1, 1) \\
D_{1\_lat} &= [0]_{7\times 1}, D_{2\_lat} = [0]_{7\times 2}
\end{aligned}
\tag{12}
$$

Using the LMI-based H_∞ control methodology [10], the calculated state-feedback gain matrices of the longitudinal and lateral formation controllers are given by (13).

$$
\begin{aligned}
K_{long} &= \begin{bmatrix}
0.0455 & -0.1056 & 0.0890 & 4.7866 & 0.4322 & -0.0002 \\
-0.1487 & -0.0114 & 0.0094 & 0.2249 & -0.0716 & -0.0008 \\
-0.0055 & -0.1031 & & & & \\
0.3373 & -0.0131 & & & &
\end{bmatrix} \\
K_{lat} &= \begin{bmatrix}
0.0157 & 0.0119 & -0.0746 & 0.0970 & 0 & 0.0481 & -0.0146 \\
-0.0131 & -0.0081 & 0.0719 & -0.0166 & 0 & -0.063 & -0.0026
\end{bmatrix}
\end{aligned}
\tag{13}
$$

Furthermore, the longitudinal and lateral compensators were designed heuristically to eliminate the corresponding formation error, and are listed in Table II.

TABLE II
PI PARAMETERS OF ALL THE COMPENSATORS

Lateral compensators			Longitudinal compensators		
Variables	K_p	K_i	Variables	K_p	K_i
ϕ	1.0	2.0	H	0.13	0.7
ψ	0.5	2.0	V	0.4	0.25
ε_{lat}	0.15	3.80	ε_{long}	0.5	4.0

To perform the computer simulations and evaluate the performance of the proposed formation control strategy, the nonlinear *Aerosonde* model was utilised with all the controller gains and parameters as shown previously.

B. Formation flight simulation

In the simulation, the constraints on the pitch and roll angles are given as: $\pm 20 deg$ and $\pm 40 deg$, respectively. The group of UAVs is tasked to navigate the 3D waypoints provided in Table (III) which can be generated from an online or offline path planning algorithm. The *planar projection* of the 3D manoeuvring trajectories are displayed in Fig. 5 to show the formation maintenance and changing when needed, where UAV 2 is the RV and UAV 1 and 3 are its neighbours. The altitudes, airspeeds and attitudes are shown in Fig. 6 and Fig. 7 respectively. Using (1) and Fig. 1, the formation change sequences are mathematically expressed by (14), where F_{d_A} denotes the initial formation shape, F_{d_B} illustrates the first formation change about their altitudes at $t = 0 s$, and F_{d_C} indicates the new longitudinal and lateral formation changes at $t = 200 s$.

TABLE III
WAYPOINTS OF UAVS FORMATION MANOEUVRE

Number	1	2	3	4	5
East(m)	0	2500	3500	500	-500
North(m)	0	600	3500	3500	1000
Altitude(m)	800	1100	1400	1400	1200

$$
\begin{aligned}
F_{d\_A} &= \begin{bmatrix} -150 & -150 & 0 \\ 0 & 0 & 0 \\ -150 & 150 & 0 \end{bmatrix} \Rightarrow F_{d\_B} = \begin{bmatrix} -150 & -150 & \mathbf{100} \\ 0 & 0 & 0 \\ -150 & 150 & \mathbf{-100} \end{bmatrix} \\
\Rightarrow F_{d\_C} &= \begin{bmatrix} \mathbf{-300} & \mathbf{-250} & 100 \\ 0 & 0 & 0 \\ \mathbf{300} & \mathbf{450} & -100 \end{bmatrix}
\end{aligned}
\tag{14}
$$

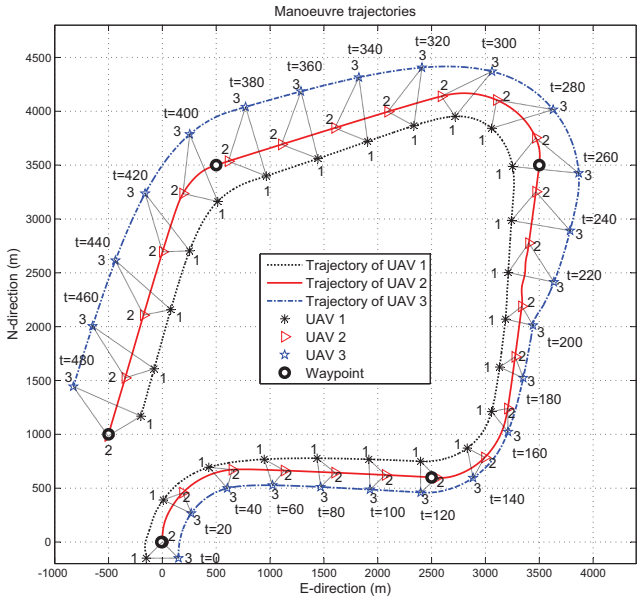

Fig. 5. Planar projection of 3D manoeuvring trajectories

As depicted, the following observations could be made:

1) The group of UAVs completed the desired manoeuvring task of tracking all the required waypoints. Furthermore, the overall formation remained stable, and small formation errors existed only during the formation change and turning manoeuvres.

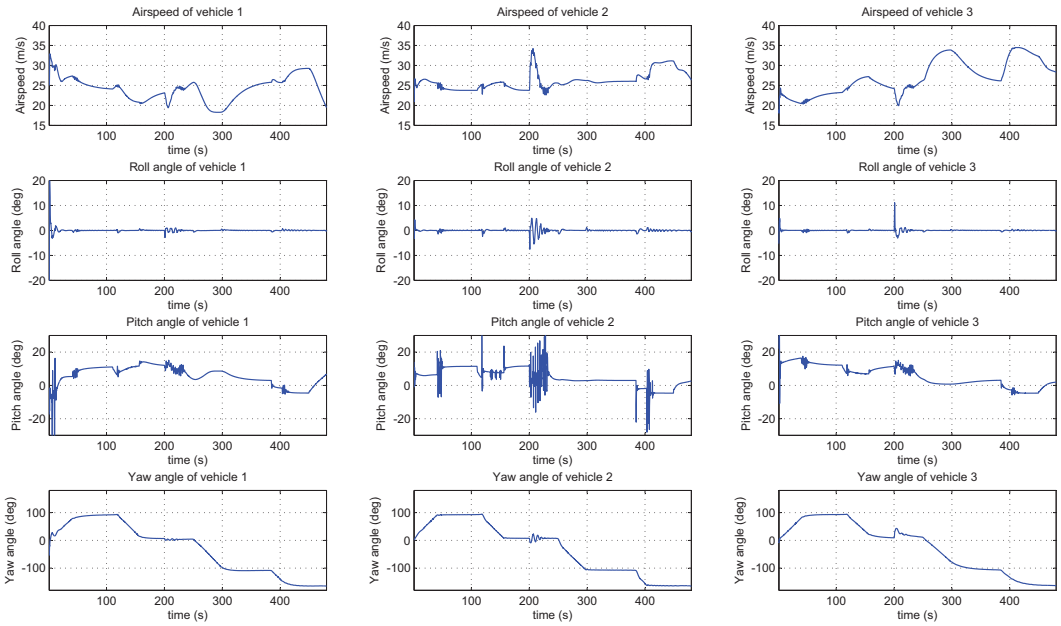

Fig. 7. Dynamics of attitudes while manoeuvring

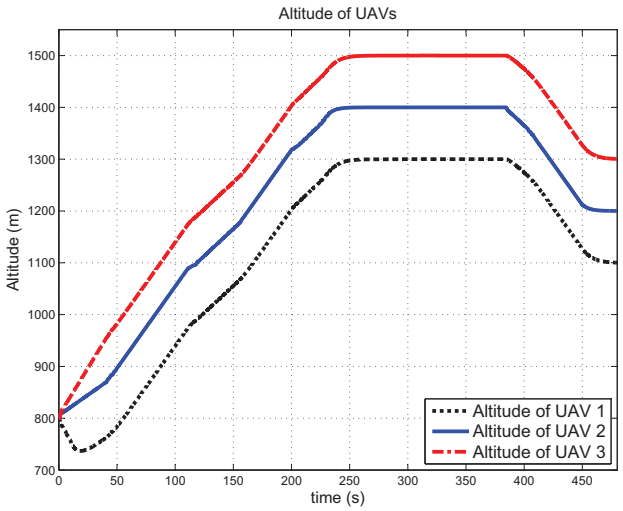

Fig. 6. Dynamics of altitudes while manoeuvring

2) During the turnings, it is clear that the attitude (pitch and roll) of each UAV remains within the specified constraints.
3) The airspeed variation with the formation changing could be observed as it was required to maintain the position of UAVs within the new desired formation as quickly as possible.

VI. Concluding Remarks

In this paper, the extension-decomposition-aggregation (EDA) scheme was extended to support the design of the decentralised autopilots for the formation flight of UAVs in 3-D. Longitudinal and lateral formation compensators were employed to eliminate the corresponding steady-state formation error. Simulation studies have been performed to verify the feasibility and effectiveness of the EDA-based formation flight strategy. Future work includes mathematical stability analysis of the overall formation and inner/outer collision avoidance.

Acknowledgment

This work was supported by the EPSRC under UK-China Science Bridge grant EP/G042594/1 and China Scholarship Council.

References

[1] M. J. Vachon, R. J. Ray, K. R. Walsh, and K. Ennix, "F/A-18 performance benefit measured during the autonomous formation flight project," in *Technical report NASA/TM-2003-210734*, NASA Dryden, Edward, CA, 2003.
[2] H. Weimerskirch, J. Martin, Y. Clerquin, P. Alexandre, and S. Jiraskova, "Energy saving in flight formation," *Nature*, vol. 413, pp. 697–698, 2001.
[3] T. Balch and R. Arkin, "Behavior-based formation control for multi-robot teams," *IEEE Transactions on Robotics and Automation*, vol. 14, pp. 926–939, 1998.
[4] J. R. T. Lawton, R. W. Beard, and B. J. Young, "A decentralized approach to formation maneuvers," *IEEE Transactions on Robotics and Automation*, vol. 19, no. 6, pp. 933–941, 2003.
[5] Y. Gu, B. Seanor, G. Campa, M. R. Napolitano, L. Rowe, S. Gururajan, and S. Wan, "Design and flight testing evaluation of formation control laws," *IEEE Transactions on Control Systems Technology*, vol. 14, no. 6, pp. 1105–1112, 2006.
[6] N. Li and H. Liu, "Formation UAV flight control using virtual structure and motion synchronization," in *Proceeding American Control Conference, Seattle, Washington, USA*, June 11-13 2008, pp. 1782–1787.
[7] A. Yang, W. Naeem, G. W. Irwin, and K. Li, "Novel decentralised formation control for unmanned vehicles," in *IEEE Intelligent Vehicles Symposium (IV 2012), in Alcalá de Henares, Spain*, June 2012, accepted.
[8] M. Chilali and P. Gahinet, "H_∞ design with pole placement constraints: an LMI approach," *IEEE Transactions on automatic control*, vol. 41, no. 3, pp. 358–367, 1996.
[9] C. Scherer, P. Gahinet, and M. Chilali, "Multiobjective output-feedback control via LMI optimization," *IEEE Transactions on automatic control*, vol. 42, no. 7, pp. 896–911, 1997.
[10] D. D. Šiljak and D. M. Stipanović, "Robust stabilization of nonlinear systems: The LMI approach," *Mathematical Problems in Engineering*, vol. 6, pp. 461–493, 2000.
[11] *AeroSim aeronautical simulation block set V1.2, users guide*, Unmanned Dynamics, 2003.